Journal of Power Sources 328 (2016) 65–74

Contents lists available at ScienceDirect

Journal of Power Sources

journal homepage: www.elsevier.com/locate/jpowsour

A novel Ni/ceria-based anode for metal-supported solid oxide fuel cells

Veronika A. Rojek-Wöckner [a], Alexander K. Opitz [b, c], Marco Brandner [a], Jörg Mathé [d], Martin Bram [e, f, *]

[a] Plansee SE, Innovation Services, 6600 Reutte, Austria
[b] Christian Doppler Laboratory for Interfaces in Metal-Supported Energy Converters, Getreidemarkt 9/164, 1060 Vienna, Austria
[c] TU Wien, Institute of Chemical Technologies and Analytics, Getreidemarkt 9/164-EC, 1060 Vienna, Austria
[d] AVL List GmbH, Hans-List-Platz 1, 8020 Graz, Austria
[e] Christian Doppler Laboratory for Interfaces in Metal-Supported Energy Converters, 52425 Jülich, Germany
[f] Forschungszentrum Jülich, Institute of Energy and Climate Research, IEK-1: Materials Synthesis and Processing, 52425 Jülich, Germany

HIGHLIGHTS

- Novel anode concept for solid oxide fuel cells based on Ni/GDC.
- Proof of function on symmetrical cells.
- Successful implementation into a metal-supported solid oxide fuel cell.
- Maximum power density 0.88 Wcm^{-2} at 850 °C with dry hydrogen.
- Impedance studies in H_2/H_2O and $H_2/H_2O/H_2S$ atmospheres.

ARTICLE INFO

Article history:
Received 26 April 2016
Received in revised form
20 June 2016
Accepted 21 July 2016

Keywords:
Cermet anode
Ceria
SOFC
Metal-supported fuel cell
Impedance spectroscopy
Sulfur poisoning

ABSTRACT

For optimization of ageing behavior, electrochemical performance, and sulfur tolerance of metal-supported solid oxide fuel cells a new anode concept is introduced, which is based on a Ni/GDC cermet replacing the established Ni/YSZ anodes. In the present work optimized processing parameters compatible with MSC substrates are specified by doing sintering studies on pressed bulk specimen and on real porous anode structures. The electrochemical performance of the Ni/GDC anodes was characterized by means of symmetrical electrolyte supported model-type cells. In this study, three main objectives are pursued. Firstly, the effective technical realization of the Ni/GDC concept is demonstrated. Secondly, the electrochemical behavior of Ni/GDC porous anodes is characterized by impedance spectroscopy and compared with the current standard Ni/YSZ anode. Further, a qualitative comparison of the sulfur poisoning behavior of both anode types is presented. Thirdly, preliminary results of a successful implementation of the Ni/GDC cermet into a metal-supported single cell are presented.

1. Introduction

Compared to conventional anode-supported solid oxide fuel cells (ASCs) metal-supported cells (MSCs) offer various potentials like lower production costs and improved ruggedness, which make them attractive for mobile applications such as auxiliary power units (APUs) [1,2]. The metallic substrate, however, requires specific adaption of solid oxide fuel cell (SOFC) processing technologies since sintering of functional layers at high temperatures under oxidizing atmosphere is restricted to avoid oxidation of the substrate [3,4]. This change in sintering conditions has tremendous effects on the properties of used materials and consequently on the electrochemical behavior of MSCs. Therefore, the achievements from ASC research can only be transferred in minor parts to the fabrication of metal supported SOFCs, making fundamental research on this promising type of fuel cells highly important.

The presented work aims at optimizing Plansee's current state-

* Corresponding author. Forschungszentrum Jülich, Institute of Energy and Climate Research, IEK-1: Materials Synthesis and Processing, 52425 Jülich, Germany.
E-mail address: m.bram@fz-juelich.de (M. Bram).

http://dx.doi.org/10.1016/j.jpowsour.2016.07.075
0378-7753/

of-the-art MSC by specifically manipulating selected components of the cell. The basis of the MSC is a porous sintered substrate with a thickness of 0.3–1 mm, which is a product of powder metallurgy starting from mechanically alloyed ITM powders (ITM = Fe26Cr(-Mo,Ti,Y_2O_3) The cross section of Plansee's state-of-the-art MSC is sketched in Fig. 1. A diffusion barrier layer (DBL-1) with a thickness of ~0.5 μm is applied on the metallic substrate by magnetron sputtering. DBL-1 is made of gadolinia-doped ceria $Ce_{1-x}Gd_xO_{2-\delta}$ (GDC).

On top of DBL-1, a bi-layered intermediate structure made of Ni/YSZ composite is deposited by screen printing. Afterwards, the electrochemically active anode layer containing the same materials is applied again by screen printing and subsequently sintered in hydrogen atmosphere. Pore size and surface roughness are reduced from bottom to top by decreasing the particle size. Furthermore, the Ni/8YSZ ratio is changed from 60/40 wt% in the first two intermediate layers to 80/20 wt% in the active anode. Enhancing the Ni content in the top layer is rather uncommon but necessary to obtain a surface quality, which is absolutely essential for achieving a dense electrolyte in the subsequent coating step. As a disadvantage, the electrochemical performance of this anode layer is lowered due to the reduction of the triple-phase-boundary (TPB) length compared to standard ASC anodes (anode-supported cell, ratio usually 60/40 wt%) [6]. Furthermore, the high Ni content of the active anode layer makes it more susceptible to sulfur poisoning and Ni coarsening [7]. Afterwards, a thin-film electrolyte with a thickness of 4–5 μm is deposited by an innovative physical vapor deposition process as described elsewhere [8,9]. Another GDC diffusion barrier layer (DBL-2) with a thickness of ~0.5 μm is deposited on the electrolyte by magnetron sputtering [10]. Finally, the electrochemically active LSCF ($La_{1-x}Sr_xCo_{1-y}Fe_yO_{3-\delta}$) cathode layer is coated on DBL-2 by screen printing. Owing to the instability of LSCF in reducing atmosphere – which is, however, necessary to prevent the metal substrate from oxidation – the cathode layer is not sintered but rather in-situ activated upon the first heat-up before fuel cell operation.

Since the electrochemical performance of current MSCs is still lower than of state-of-the-art anode-supported fuel cells, and since MSC specific degradation phenomena are still not fully understood, fundamental research on MSC-related issues is urgently needed [3,4]. One of the current main challenges is the development of an anode layer that can be sintered under reducing atmospheres and which is less prone to degradation phenomena. To achieve these desired improvements, the introduction of new anode materials is frequently discussed in literature and as a very promising approach the substitution of YSZ by acceptor doped ceria is suggested [1,11–13]. A large benefit of ceria-based anodes is the fact that under reducing conditions ceria becomes a mixed ionic and electronic conductor, which enables large parts of the ceria surface to contribute to the electrochemical reaction [14,15].

Therefore, the main goal of the present study is the development of a novel cermet anode for metal-supported SOFCs, which is based on Ni/GDC and replaces exclusively the topmost anode layer (layer 2c in Fig. 1). Layers 2a and 2b will not be replaced by Ni/GDC to keep the related changes in mechanical stability and thermal expansion as small as possible. Since electrochemical reaction is expected to take mainly place in layer 2c, we currently do not see the need of adapting these layers as well. Achieving the main goal will be pursued by the following steps: (i) Characterization of the sintering behavior of Ni/GDC under reducing conditions. (ii) Establishing a processing route for real porous Ni/GDC based cermet anodes. (iii) Electrochemical characterization of this novel anode by means of impedance spectroscopy on model-type anode samples and comparison with the current state-of-the-art Ni/YSZ. (iv) Introduction of the Ni/GDC anode into a real MSC and preliminary electrochemical characterization of the cell performance.

2. Experimental and methods

As ceramic powders GDC (CeO_2 doped with 10 mol% Gd_2O_3, d_{50} = 0.35 μm, specific surface area = 7.62 $m^2\ g^{-1}$) and YSZ (ZrO_2 stabilized with 8 mol% Y_2O_3, d_{50} = 0.58 μm, specific surface area = 11.61 $m^2\ g^{-1}$) were used.

For sinter studies the ceramic powders were compacted at a pressure of 150–250 MPa into cylindrical samples (d = Ø25 mm, h ≈ 4 mm, m = 3–4 g), using an automated press (KOMAGE Gellner KG, Germany). Subsequently, the samples were sintered in H_2 atmosphere at temperatures between 1000 °C and 1300 °C for 3 h (heating rates were 3 K min^{-1}). The sintering temperatures were chosen to provide an overview of the sintering behavior above and below standard sintering temperature of 1200 °C. Then, the linear changes in geometry were measured to obtain information about the shrinkage behavior.

For screen printing of electrodes, a paste was prepared from the ceramic powders as used for the sintering study and metallic nickel powder (Ni, d_{50} = 1.73 μm) aiming at different Ni/ceramic ratios (80/20 wt% and 60/40 wt%). The liquid component of the paste was based on ethyl cellulose (45 cps, 4 to 8 wt%) dissolved in terpineol as binder with commercial dispersing agent (0.2–0.4 wt% Nuosperse FA196, Elementis Specialities, USA). Ni/GDC pastes were prepared accordingly to the Ni/YSZ state-of-the-art paste [3], whereas adjustments of the solid content (55 wt% to 70 wt%) were based on rheological optimizations.

With these anode pastes free standing Ni/YSZ and Ni/GDC anode layers were screen printed on transfer paper (Rullis Russer Coaters Limited, England) utilizing a semi-automated screen printer (Ekra 2, Asys Group, Germany). The samples were dried at 60 °C for 1 h. The layer was detached from the paper in warm water and dried for 20 min at room temperature. Round samples with different diameters (ø 9, 14, 22 mm) were die-cut and the samples were sintered on a powder bed varying the temperature in the range of 1000 °C–1300 °C, for 3 h in H_2 atmosphere. The shrinkage was calculated from the change in diameter.

To investigate the microstructure of the novel electrodes, anode layers (2c, Fig. 1) were also screen printed on a porous state-of-the-art MSC substructure (i.e. consisting of layers 1–2b in Fig. 1), dried at 60 °C and sintered within a temperature range of 1100 °C–1300 °C for 3 h in H_2 atmosphere.

For electrochemical characterization symmetrical electrolyte-supported samples were prepared. Therefore, a matrix of 2 × 2 anode layers (9 × 9 mm^2 each) were screen printed on both sides of 8YSZ-electrolyte films (37.5 × 37.5 mm^2, d = 150 μm ± 15 μm, Kerafol GmbH, Germany). Subsequently the samples were laser-cut to 1 × 1 cm^2 cells and sintered at 1100 °C (Ni/GDC) or 1200 °C (Ni/YSZ) for 3 h in H_2.

For impedance measurements the symmetrical anode samples were mounted between soft Ni-meshes, which were contacted by Pt sheets and connected to the impedance interface by Pt wires. For simulating SOFC anode conditions a gas with ~2.5% H_2/~2.5% H_2O/balance Ar was fed through the experimental setup with a flux of about 3 Lh^{-1} [16]. The electrochemical polarization resistances of the anodes were characterized by impedance measurements (PSM 1753 with IAI interface, Newton's Fourth Ltd., UK) in a frequency range between 1 MHz and 10 mHz with an ac voltage of 20 mV (rms). The measurements were conducted under open-circuit conditions (i.e. without an applied bias) and operating temperatures ranging from 650 °C to 850 °C. For sulfur contamination, H_2S was fed to the fuel gas flow by adding appropriate amounts of a H_2S premix (2.5% H_2/200 ppm/balance Ar) to the feed gas stream.

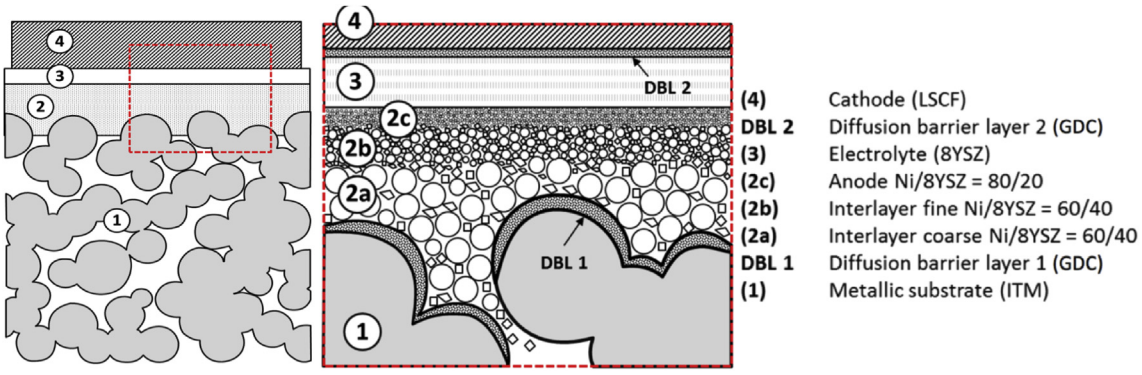

Fig. 1. Schematic of Plansee's MSC representing the current status of development [4,5].

Entire MSCs with an active cell area of 16 cm^2 with Ni/GDC anodes were manufactured analogously to the state-of-the-art cell (see Fig. 1), excluding the layer 2c, which was replaced by the novel Ni/GDC cermet. A detailed description of the processing steps of the state-of-the-art cell and the progress in cell development can be found elsewhere [5,17,18]. The anode was processed identical to those shown in Fig. 1 (see above). The Ni/GDC layer thicknesses were 6 μm (cell#1) and 3 μm (cell#2). Before electrochemical characterization a heating and activation procedure was performed including dwell times for crystallization of the glass seal at 350 °C and in-situ sintering of the cathode at 850 °C. A commercial glass seal (Schott AG, G018-311, Germany) was used for sealing. A standard LSCF cathode material ($La_{0.6}Sr_{0.4}Co_{0.2}Fe_{0.8}O_{3-\delta}$ [5]) was used for the cell tests. Subsequently, I-V-curve measurements were conducted under dry and moist conditions between 650 °C and 850 °C. For recording dc data the current was ramped with 40 $mA^{-1}$and the working point for measurement of the electrical power output was defined at 0.7 V.

3. Results and discussion

3.1. Sintering of ceramic powder compacts

A non-dilatometry sintering study was done on compacted powder specimen in H_2 atmosphere to estimate the sintering behavior of GDC in comparison to YSZ, under fully reducing atmosphere and real processing parameters (3 $Kmin^{-1}$ heating rate, 3 h dwell time). The shrinkage of pure GDC and YSZ samples (i.e. without any Ni added) is depicted in Fig. 2 (a) as a function of dwell temperature. The plotted shrinkage was evaluated by calculation of the linear shrinkage behavior of pellets by measuring their change in diameter.

The results reveal that in H_2 the sintering activity of GDC is significantly higher compared to YSZ for temperatures lower than 1100 °C. Obviously, already at 1000 °C the GDC specimen (green density $\rho_{rel} = 62\%$) is subjected to strong relative shrinkage by approx. -11%. The total densification of GDC only slightly changes in the temperature range between 1200 °C and 1300 °C, approaching approximately −12% for 1300 °C (final relative density $\rho_{1300°C} \approx 90\%$). The sintering activity of YSZ appears to strongly increase for temperatures above 1100 °C. Concluding from these results, the shrinking process of GDC in reducing atmosphere already starts at a lower temperature than 1000 °C and the initial and intermediate stage of sintering may be observed only to a marginal extent in the here given temperature range. The presented temperature range covers the initial and intermediate stage of the sintering process of YSZ in reducing atmosphere. Also, slight anisotropic shrinkage behavior for both ceramics is observed, because the change in diameter is higher than the change in height of the powder compact. This anisotropy is probably caused by density gradients occurring during uniaxial pressing.

A different sintering behavior of GDC compared to YSZ was expected in H_2 atmosphere with respect to related literature [19]. Thus, during the sintering process of GDC different sintering mechanisms (i.e. oxygen removal) may become relevant, which can dominate the shrinkage behavior of GDC especially in reducing atmosphere. In other studies, found in literature, the difference in sintering is explained by atmosphere-dependent viscoelastic properties of GDC ceramics [20,21]. Accordingly, in reducing atmosphere, electronic defects are generated in the GDC lattice by the reduction of Ce^{4+} to Ce^{3+}. This phenomenon plays an important role in the thermally activated cation diffusion and leads to higher shrinkage rates [22].

Less discussed in literature so far is the investigation of the phase stability of GDC in the Ni/GDC anode cermet if sintered under reducing atmospheres. In this regard, X-ray diffraction studies were conducted on compacted powder specimen. Under the given conditions no significant influence of sintering temperature or reducing sintering atmosphere on the phase stability of neither GDC nor Ni is observed, as shown in Fig. 2 (b) [16].

3.2. Non-constrained shrinkage of cermet material

Plansee's state-of-the-art MSC anode is a Ni/YSZ-anode with a metal-ceramic ratio of 80/20 wt%. Considering the mixed conductivity and improved sintering activity of GDC compared to YSZ, the Ni/GDC ratio was reduced to 60/40 wt% in the subsequent sintering study, which was done on free-standing anode layers to investigate the non-constrained sintering behavior of presented cermets.

The green densities of the anode layers based on Ni/GDC and Ni/YSZ account for 60.8% and 62.8%, while the screen printing inks are loaded with 12.5 vol% and 14.7 vol% of solid content, respectively. Assuming that the free standing layers show isotropic shrinkage behavior, the linear shrinkage is calculated as the change in diameter of the circular samples.

At 1100 °C the Ni/YSZ cermet reference shows a shrinkage of approx. -3%, which increases to −15% at 1300 °C, as given in Fig. 3 ((a), black dashed line). This behavior might point to the fact that despite the low ratio, YSZ dominates the shrinkage behavior in Ni/YSZ due to a phenomenon in literature referred to as pinning effect [23].

However, comparing the non-constrained shrinkage of Ni/GDC 60/40 wt% Fig. 3 ((a), red dot-dashed line), a significant difference to the reference and less similarity to shrinkage of pure GDC is observed. As discussed above, shrinkages of −11 to −12% were measured between 1000 and 1300 °C for the compact, whereas the

free standing layer only shrinks by −6% at 1000 °C. With increase of temperature, the shrinkage strongly increases and approaches a value of about −17% at 1300 °C for the Ni/GDC cermet, which is in contrast to powder compacts of pure GDC (see above). Those results suggest that on the one hand the addition of metallic Ni moderates the shrinking of GDC at lower temperature, but on the other hand, Ni/GDC anodes still need to be sintered at lower temperatures than the Ni/YSZ standard anode to counteract the stronger sintering activity of GDC and Ni at high temperatures.

3.3. Microstructural evaluation of Ni/GDC anode layers

Since SEM sample preparation of free standing Ni/GDC layers was not successful, a microstructural investigation was done on a Ni/GDC anode, which was supported by a MSC standard substrate, consisting of a porous ITM substrate (layer 1) covered with two Ni/YSZ interlayers (layers 2a and 2b) as sketched in Fig. 1. The SEM images of cross-sections of differently prepared anodes are given in Fig. 3 (b).

The cross-sections of the Ni/YSZ and Ni/GDC anodes with different ceramic to metal ratios support the data of sintering experiments above. A Ni/GDC anode with a ratio of 80/20 wt% sintered at 1200 °C showed the expected strong coarsening of Ni particles and highly reduced porosity of the layer, which both drastically decrease the catalytically active surface (see top right image of Fig. 3 (a)). A reduction of the Ni-content to 60% resulted in a slightly reduced Ni grain growth, but still the available surface is unsatisfactorily low (cf. bottom right image in Fig. 3 (b)). To further limit Ni grain growth, the sintering temperature was lowered. From the results in Fig. 3a a temperature between 1000 and 1100 °C is expected to yield a sintering behavior similar to the current state-of-the-art anode. However, since not only the shrinkage of the anode layer itself is important, but also a sufficient bonding to the Ni/YSZ interlayer (cf. layers 2a and b in Fig. 1) is needed a sintering temperature of 1100 °C was chosen for novel Ni/GDC anodes. The resulting microstructure found in an anode with a Ni/GDC ratio of 60/40 wt%, which was sintered at 1100 °C for 3 h in H_2 is shown in the bottom left SEM image in Fig. 3. The obtained morphology is highly promising from two point of views: (i) The surface is rather smooth and the pore sizes close to the surface are small enough to ensure a dense growth of a PVD deposited electrolyte for preparation of complete cells (results of cell tests see below). (ii) The Ni/GDC ration of 60/40 instead of 80/20 potentially allows for a larger TPB-length and GDC surface area to ensure a higher electrochemical activity of the anode. Especially the latter will be discussed in detail in the following sections.

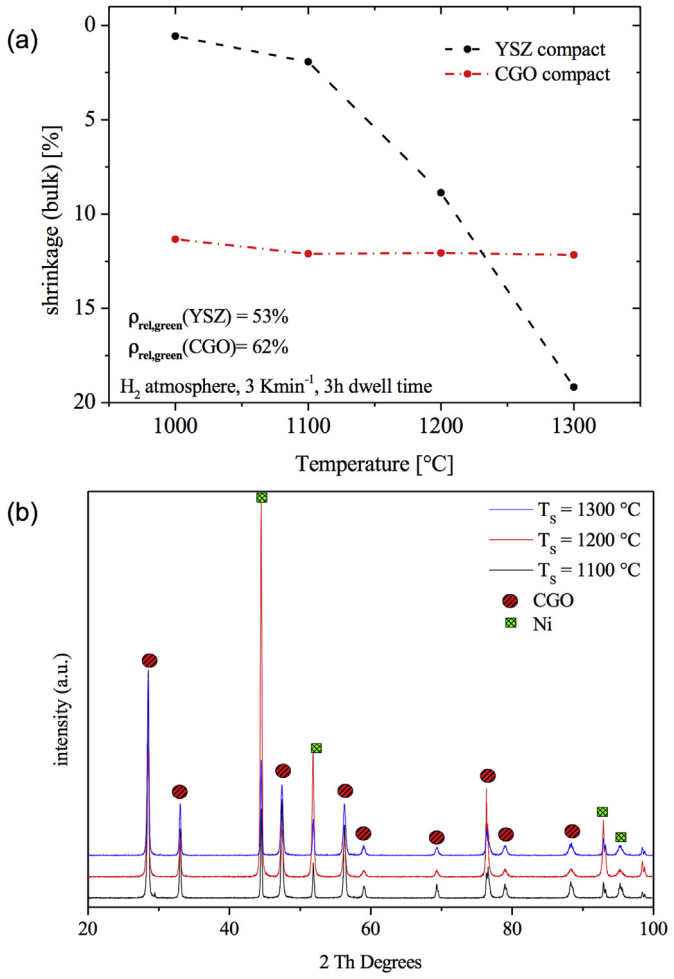

Fig. 2. **(a)** Shrinkage of compacted ceramic powder specimen plotted versus dwell temperature. **(b)** X-ray powder diffraction pattern of Ni/GDC 60/40 wt% compacted specimen in a temperature range of 1100 °C–1300 °C.

3.4. Electrochemical impedance spectroscopy on symmetrical model-type samples

Since from a microstructural point of view Ni/GDC 60/40 wt% sintered at 1100 °C was specified as best choice anode, a systematic study of electrochemical anode performance was conducted by means of impedance spectroscopy on electrolyte supported symmetrical anode samples. Impedance spectra measured on novel Ni/GDC anodes are depicted in Fig. 4 (a). The high frequency intercept in the Nyquist plot consists of contributions from an ionic transport resistance in the electrolyte and to a minor degree of an electronic current collection resistance and possible contact resistances [24]. The temperature dependence of the high frequency intercept is as expected for ionic transport resistance in the electrolyte and the corresponding ionic conductivity is in accordance with literature data [25]. Moreover, from the ionic conductivity of the electrolyte a temperature was calculated [26,27]. These temperature values were in sufficient agreement with the temperatures measured by a type K thermocouple in the experimental setup. Thus, the current distribution in the electrolyte can safely be assumed to be homogeneous and a laterally inhomogeneous polarization of the electrode (e.g. originating from insufficient current collection) can safely be neglected.

The medium and low frequency feature are assigned to polarization processes of the porous anode and the capacitive contribution to the low frequency arc is mainly attributed to the chemical capacitance of GDC [25,27–29]. In the following, the total resistance of both features is denoted as polarization resistance of the Ni/GDC cermet anode. From the impedance spectra in Fig. 4 (a) and with the projected area of ca. 0.8 cm^2 an area specific resistance (ASR) of 0.41 Ωcm^2 at 759 °C can be extracted for one porous anode, which is in good accordance to related anode systems in literature [25]. Further details regarding the origin and/or the nature of the individual electrode processes will be discussed below.

For reasons of comparison, impedance measurements were also conducted on electrolyte supported symmetrical samples with Plansee's current standard Ni/YSZ 80/20 wt% anode [3]. Impedance spectra measured under the same conditions as Ni/GDC are shown in Fig. 4 (b). They also consist of a high frequency axis intercept and at least two contributions at medium and low frequencies. The high frequency feature shows virtually the same behavior as in case of Ni/GDC electrodes and is thus also attributed to an ion transport resistance in the electrolyte as well as possible current collection

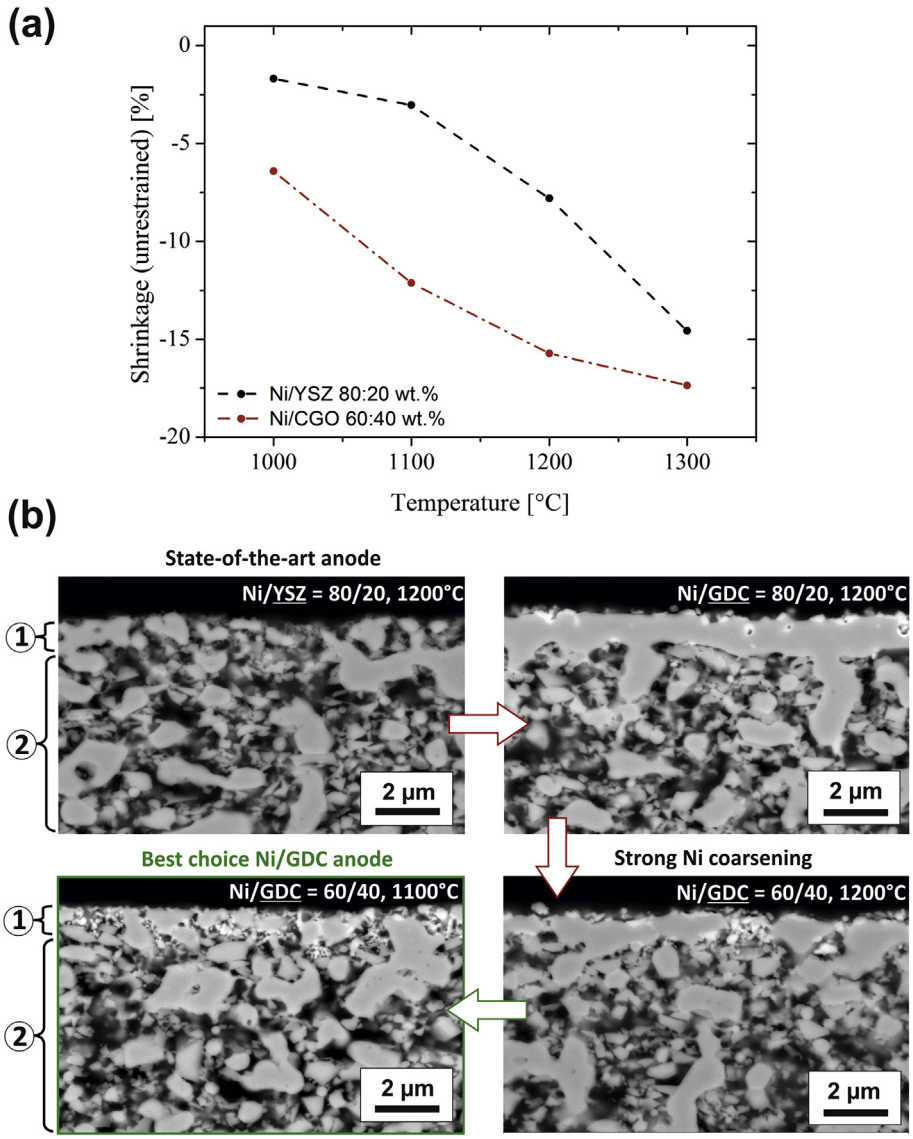

Fig. 3. **(a)** Non-constrained shrinkage investigated on free standing anode layers (sintering done in H_2, heating rate 3 $Kmin^{-1}$, 3 h dwell time). **(b)** SEM cross sections of MSC anodes with Ni/YSZ 80/20 wt%, Ni/GDC 80/20 wt% and 60/40 wt%. The different layers were prepared on identical porous Ni/YSZ supports: (1) Anode (2) Interlayer Ni/YSZ. The cermets were sintered at 1100 °C or 1200 °C for 3 h in H_2.

and contact resistances. The medium and low frequency features are attributed to electrode processes. Interestingly, the peak frequency of the low frequency semi-circle does virtually not change upon temperature variation and stays always between 25 and 40 Hz. Further details regarding temperature dependencies and discussion of possible elementary processes will be given below.

For data analysis the impedance spectra obtained on both types of electrodes were parameterized by a complex non-linear least squares fit (software: Z-view, Scribner Associates, USA). For this means, the equivalent circuit shown in Fig. 4 (c) was used for both Ni/GDC and Ni/YSZ spectra – therein R and CPE denote resistors and constant phase elements, respectively. The impedance of a constant phase element Z_{CPE} is defined as $Z_{CPE} = 1/[(i\omega)^n Q]$ with i and ω being imaginary unit and angular frequency, respectively; n and Q are fitting parameters. It should be noted that the equivalent circuit was only used for parameterization of the spectra and does not correspond to a specific reaction mechanism. Rather, the resistor denoted R_{HF} considers the high frequency intercept and the two R-CPE elements are used to fit the two arcs, which can be observed in the electrode features of both electrode types. Moreover, the reader should note that the use of the same circuit for both electrode types should neither imply a similarity in the reaction mechanism on the different materials nor suggest the possibility of a quantitative comparison of elementary processes (e.g. normalizations based on the Ni content or TPB length). Especially the latter would require a highly non-trivial evaluation of the electrode's geometry parameters, which would go far beyond the scope of the present study.

3.5. Temperature dependence of electrode processes

The resistors R_{MF} and R_{LF} obtained from CNLS-fits as well as the total polarization resistance $R_{pol} = R_{MF} + R_{LF}$ were related to the nominal area (0.8 cm^2) of one porous electrode. The obtained area specific resistances are shown as a function of temperature in the Arrhenius diagrams in Fig. 5.

As can be seen from Fig. 5 (a) and (b), the low frequency feature of both electrode types shows only very weak (if any) temperature

dependence. The mean activation energies of $1/R_{LF}$ obtained from all measured samples are 0.13 ± 0.06 eV and ≈0 eV for Ni/GDC and Ni/YSZ, respectively. Since neither on Ni/GDC nor on Ni/YSZ model systems such low activation energies were observed for an electrochemical elementary step, this process may be most likely interpreted as a kind of gas transport limitation [14,30–33]. In accordance with such an interpretation, the pore sizes in Ni/GDC and Ni/YSZ electrodes are relatively small – see SEM images in Fig. 6 (a) and (b), respectively. From kinetic gas theory the critical pore size can be estimated by calculating the mean free path λ of H_2 by

$$\lambda_{H_2} = \frac{k_B T}{\sqrt{2}\pi d^2 p} \quad (1)$$

Therein k_B, T, p, and d denote Boltzmann's constant, absolute temperature, pressure, and diameter of a H_2 molecule. Assuming H_2 to be a sphere with a diameter of 0.3–0.25 nm, Equation (1) for a temperature of 800 °C and a total pressure of 1 bar yields a mean free path in the range of 370–530 nm. Since most of the pore diameters of both cermets in Fig. 6 are significantly below 500 nm, a gas diffusion limitation appears to be a very reasonable explanation for both low frequency processes.

In contrast to the almost temperature independent low frequency process, the medium frequency process appearing on both electrode types, exhibits a clear temperature dependence (see Fig. 5 (b) and (c)). The activation energies of $1/R_{MF}$ are 0.93 ± 0.07 eV in case of the Ni/GDC anodes and 1.04 ± 0.11 eV for Ni/YSZ. This resistance may be related to classical electrode processes such as charge transfer or co-limitation of adsorption and surface diffusion [25,34], but also ion transfer processes or current constriction effects at the interface of electrolyte and porous electrode can lead to resistances with the observed activation energies [35]. However, an unambiguous conclusion regarding the responsible elementary processes cannot be drawn solely from the impedance data. For a more detailed explanation of the underlying mechanisms as well as for a direct comparison of the material's electrocatalytic properties a systematic variation of both cermets in combination with measurements on model anodes (e.g. patterned thin films) is necessary. Both approaches are covered in ongoing and forthcoming studies.

In terms of total polarization resistance, the novel Ni/GDC anode outperforms the standard Ni/YSZ anode (cf. Fig. 5 (c)), despite the large contribution of the weakly activated process on Ni/GDC. This observation may be an indication for a higher optimization potential of this type of anode. It should also be noted that especially at higher temperatures the impact of the low frequency process on R_{pol} becomes significantly larger – see the shallower slopes of the curves in Fig. 5 (c) at higher temperatures. This behavior can be interpreted as an evidence for a serial connection of R_{MF} and R_{LF} or a connection in terms of a transmission line (commonly referred to as co-limitation) [36–38]. According to the above discussed results, an optimization of the electrode's porosity appears to be the most promising approach to increase the performance of both Ni/GDC and Ni/YSZ anodes. Referring to hydrogen's approximate mean free path of about 0.5 μm at SOFC operation conditions (see equ. 1 and discussion above) an increase of the pore size to a range of 0.7–1.5 μm appears to be a promising approach to significantly repress the contribution of gas diffusion limitation. A potential approach to realize such a change in microstructure without completely changing the electrode morphology is the use of pore forming additives. Moreover, a further reduction of sintering temperature could also lead to increased porosity of the Ni/GDC cermet (cf. the shrinkage behavior in Fig. 3a).

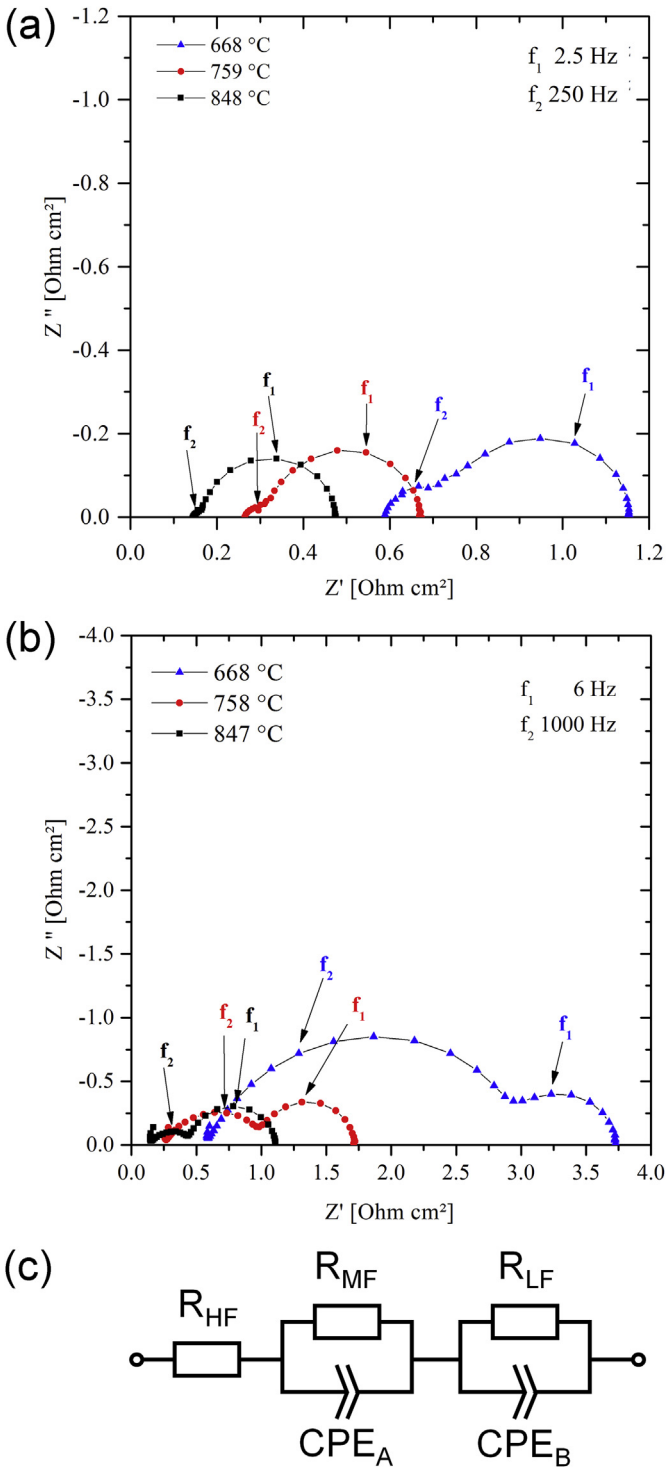

Fig. 4. **(a)** Impedance spectra (Nyquist plot) measured on a Ni/GDC cermet anode in H_2/H_2O atmosphere between 668 °C and 848 °C. **(b)** Impedance spectra (Nyquist plot) measured on a Ni/YSZ cermet anode in H_2/H_2O atmosphere between 668 °C and 847 °C. **(c)** Equivalent circuit used for CNLS-fitting of the impedance spectra.

3.6. H_2S-poisoning behavior

In order to investigate the sulfur poisoning behavior of both cermet anodes, measurements at 780 °C in $H_2/H_2O/H_2S$ atmospheres were conducted. As before, the H_2 and H_2O partial pressures were ca. 25 mbar each (balance Ar). The H_2S concentration

was 10 ppm in case of Ni/YSZ and 25 ppm for Ni/GDC electrodes. It should be emphasized, that in the present paper only a qualitative comparison of the sulfur poisoning is aimed at. A quantitative analysis of sulfur poisoning on porous anodes is highly challenging owing to the following reasons: (i) Ni/YSZ and Ni/GDC anodes need to be prepared with different Ni contents owing to their different sintering behavior (see Section 3.3). (ii) The defect-chemical properties of YSZ and GDC are strongly different. While YSZ is a pure ion conductor, GDC offers mixed ionic and electronic conductivity, leading to completely different electrochemically active regions [14,15]. For gaining more fundamental insight into sulfur poisoning we follow the approach of model experiments on micro-patterned thin film electrodes, which are published elsewhere [39]. A quantitative interpretation of resistance changes on porous anodes, is thus far beyond the scope of the present study and will be the topic of forthcoming work. The data of experiments under different H_2S concentrations were therefore not chosen with the intention to quantitatively analyze the effect of sulfur, but due to similar temperatures and time durations of the two poisoning and regeneration experiments, which allow a comparison of the significantly different response of the resistances R_{MF} and R_{LF}.

In Fig. 7 the observed evolution of R_{MF}, R_{LF}, and R_{pol} is depicted as a function of time. In case of Ni/GDC (Fig. 7a) both resistances R_{MF} and R_{LF} show a poisoning response. Upon H_2S addition, R_{LF} increases by about 50%, whereas R_{MF} only slightly grows. (A poisoning with 10 ppm H_2S leads to slightly smaller increases of the polarization resistance – not shown – and shows similar regeneration behavior, which is in good agreement with literature [11,12]). Since the addition of small amounts of H_2S cannot significantly change the gas diffusion in the pores of the cermet anode, the large change of R_{LF} is a clear indication that this process cannot exclusively be explained by gas transport limitation. A possible

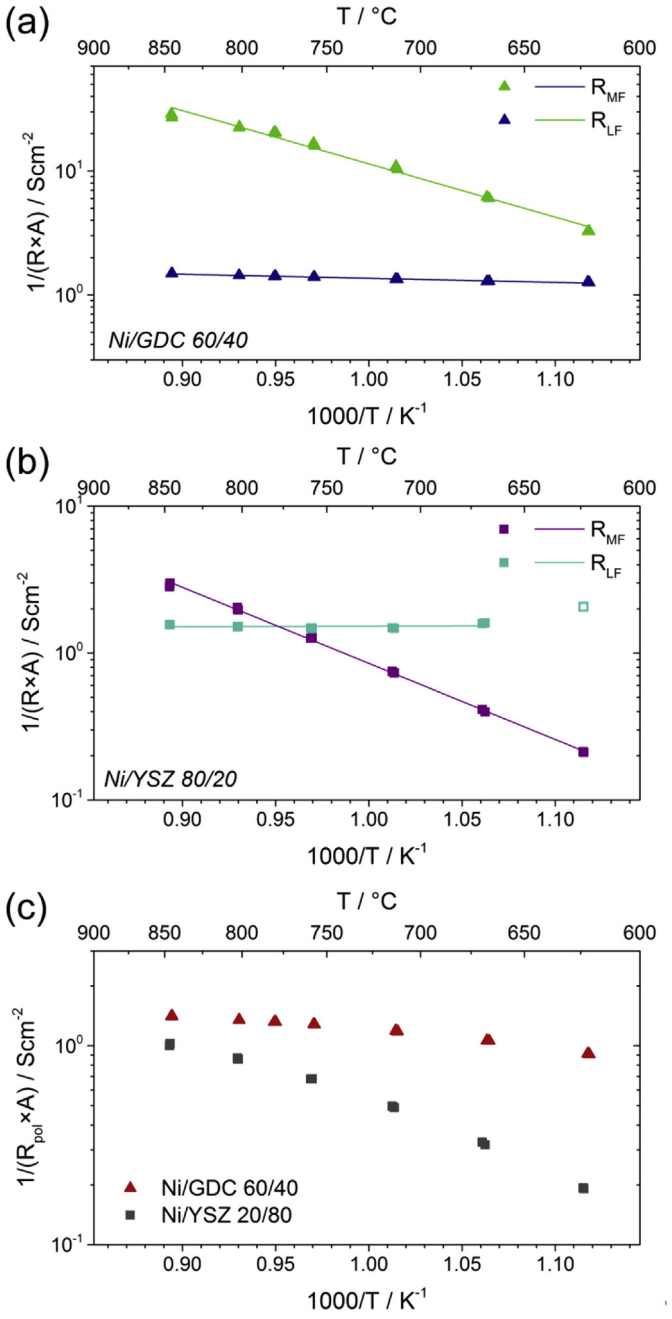

Fig. 5. Arrhenius diagrams of area specific resistances. **(a)** Resistances of medium and low frequency feature in Ni/GDC spectra. **(b)** Resistances of medium and low frequency feature in Ni/YSZ spectra. (The data of R_{LF} at ~625 °C were not considered for calculation of the activation energy due to some difficulties with the CNLS-fit.) **(c)** Comparison of total electrode polarization resistance of Ni/GDC (triangles) and Ni/YSZ (squares) anodes.

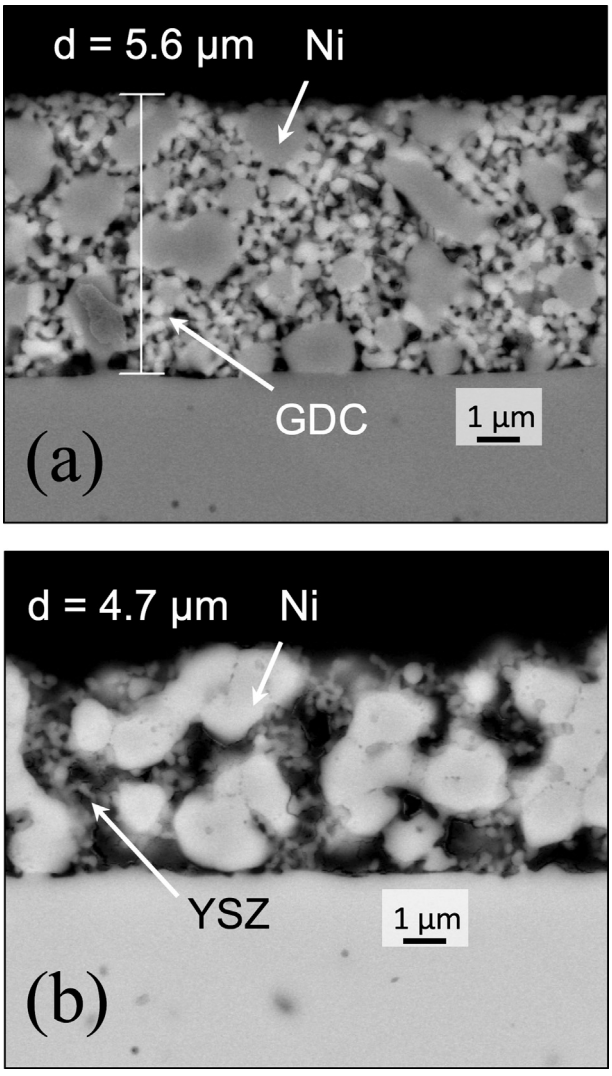

Fig. 6. SEM-image of the cross section of a corresponding Ni-GDC anode (a) and the Ni/YSZ anode (b) in the symmetrical cell model geometry.

explanation might be that R_{LF} actually consists of two contributions: a diffusion limitation and a real electrochemical process at the GDC surface or at the GDC/Ni/gas three phase boundary. Unfortunately, these processes cannot be separated in impedance measurements due to the large chemical capacitance of GDC (about 0.06 F at 780 °C). However, assuming an additional resistance being hidden in the low frequency arc of the spectra in Fig. 4 (a), this electrochemical elementary process would be even more affected by H_2S than the observed change of resistance R_{LF} in Fig. 7 (a). Another hint that R_{LF} in case of Ni/GDC indeed is a convolution of an electrochemical and a gas diffusion process is the degree of resistance increase in presence of H_2S. From sulfur poisoning experiments on thin film based GDC model-composite electrodes, which do not exhibit gas diffusion limitation at all, an increase of the electrode resistance by a factor of 2–5 is expected [39]. However, here only a 50% increase was observed on the cermet, indicating a possible gas diffusion limitation apparently attenuating the sulfur poisoning effect. The irreversible part of sulfur poisoning, which persists after stopping the addition of H_2S to the feed gas, was also observed on the GDC model composite electrodes and on model-composite electrodes an incorporation of sulfide into the GDC bulk was identified to be the most likely origin of this effect.

Interestingly, Ni/YSZ reacts completely different to the addition of H_2S to the feed gas. On this anode the low frequency feature shows no sulfur poisoning effect at all. This behavior strongly supports the above discussed interpretation of R_{LF} on Ni/YSZ being caused by gas transport limitation. The sulfur poisoning effect can exclusively be assigned to resistance R_{MF}, therefore also supporting the interpretation of a real electrochemical or electro-catalytic effect. It is also evident from Fig. 7 (b), that the poisoning effect on R_{MF} consists of a quick resistance jump and a slow degradation during measurements in H_2S containing atmosphere. The continuous degradation process appears to be even slower than in case of Ni/GDC and the poisoning is also not fully reversible upon switching back to sulfur free feed gas. A qualitatively almost identical sulfur poisoning and regeneration behavior was already observed in our study on micro-patterned Ni electrodes [40] and also in case of ASC anodes [41].

It should also be noted that for both electrode types the fluctuations of the polarization resistance with time can exclusively be attributed to the low frequency process. Reasons for this behavior cannot be interpreted unambiguously but may be due to the possibly related gas transport process in the pores of the electrode.

3.7. Implementation of Ni/GDC anodes in a single metal-supported cell

For testing the practical applicability of Ni/GDC anodes in MSCs, two metal-supported fuel cells (named cell#1, cell#2) including a novel Ni/GDC anode with an active cell area of 16 cm^2 were produced and preliminary electrochemical results will be discussed in the following.

I-V-curve measurements were conducted on two different cells under dry and moist conditions between 650 °C and 850 °C. At start of cell#2 the open circuit voltage (OCV) valued 1.063 V at 850 °C.

At 0.7 V and at 850 °C current densities of 1.27 Acm^{-2}, 1.24 Acm^{-2}, and 1.15 Acm^{-2} were measured in 0% H_2O/H_2, 5% H_2O/H_2 and 12.5% H_2O/H_2, respectively (I-V curves not shown). Changing temperature to 750 °C led to a slightly increased open circuit voltage of 1.106 V, which is in accordance with the thermodynamics of H_2 oxidation. The corresponding current-voltage curves obtained at different temperatures in dry hydrogen are depicted in Fig. 8. A summary of measured parameters is given in Table 1. The measured maximum power density of P_{max} = 0.88 W/cm^2 at 850 °C is a promising value especially when considering that a significant part

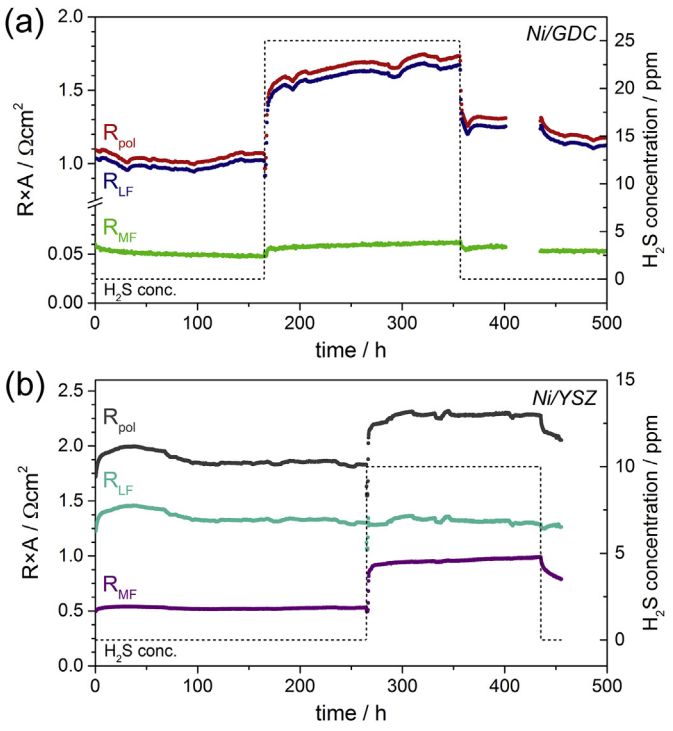

Fig. 7. **(a)** Evolution of R_{MF}, R_{LF}, and R_{pol} with and without the presence of H_2S for Ni/GDC anode and **(b)** Ni/YSZ anode. (The missing points in (a) were caused by a technical problem with the setup.).

of the anode polarization resistance is caused by a gas transport limitation, which can be lowered by optimizing the anode's microstructure (cf. Section 3.5).

So far, it is the first time that a Ni/GDC anode obtained via a particle-based route was implemented into a metal-supported SOFC yielding in very good performance [42–47].

4. Conclusions

The present study aimed at replacing the ionic conductor YSZ by the mixed conductor GDC in the state-of-the-art cermet anode for metal-supported solid oxide fuel cells, which could be successfully demonstrated by the following results:

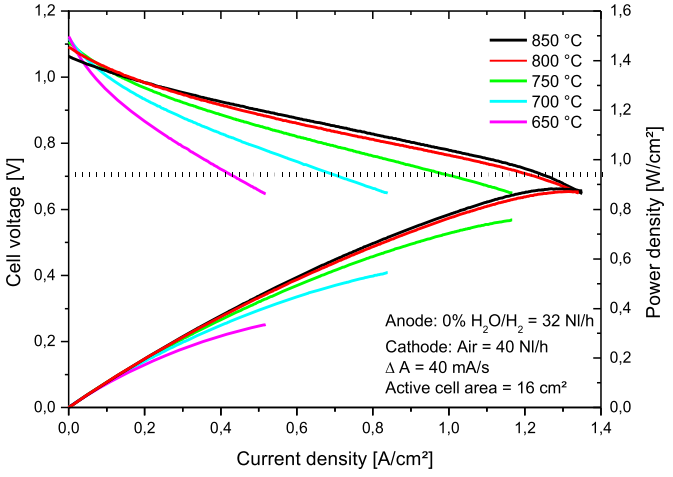

Fig. 8. Current-voltage and current-power characteristics of a single metal-supported cell employing a Ni/GDC cermet anode (cell#2).

Table 1
Summary of measured dc characteristics on a MSC with Ni/GDC anode under different conditions.

Conditions		OCV	Current densities at 0.7V	P_{max}
Cell 1[a]	800 °C; dry H_2	1.058 V	1.03 A/cm^2	0.72 W/cm^2
	700 °C; dry H_2	1.101 V	0.75 A/cm^2	0.57 W/cm^2
Cell 2[b]	850 °C; dry H_2	1.063 V	1.27 A/cm^2	0.88 W/cm^2
	850 °C; 5% H_2O/H_2	1.027 V	1.24 A/cm^2	0.87 W/cm^2
	850 °C; 12.5% H_2O/H_2	1.005 V	1.15 A/cm^2	0.84 W/cm^2
	800 °C; dry H_2	1.085 V	1.26 A/cm^2	0.89 W/cm^2
	750 °C; dry H_2	1.106 V	1.01 A/cm^2	0.76 W/cm^2
	700 °C; dry H_2	1.117 V	0.71 A/cm^2	0.55 W/cm^2
	650 °C; dry H_2	1.124 V	0.43 A/cm^2	0.52 W/cm^2

[a] Thickness of anode functional layer ca. 6 μm.
[b] Thickness of anode functional layer ca. 3 μm.

Firstly, the chemical and physical stability of GDC as well as its sintering activity in reducing atmosphere was verified by a sintering study on GDC with respect to YSZ reference. In H_2 atmosphere the shrinkage of Ni/GDC cermets was found to be significantly higher than that of Ni/YSZ cermets.

Secondly, a new processing standard for porous Ni/GDC anodes was developed. Due to the higher sintering activity of Ni/GDC the processing temperature was decreased to 1100 °C, which had the positive effect of less Ni grain growth. Consequently, the Ni content in the cermet could be optimized.

Thirdly, an impedance study in H_2/H_2O and in $H_2/H_2O/H_2S$ atmospheres was carried out on novel Ni/GDC cermet anodes as well as on standard Ni/YSZ anodes. On both systems at least two resistive contributions to the overall electrode polarization resistance were identified – one at medium and the other at low frequencies. In case of Ni/GDC the dominating low frequency resistance seems to be at least partly caused by a gas transport limitation. However, owing to its behavior in sulfur containing feed gas a second, electrocatalytic contribution is evident. The medium frequency process plays only a minor role. On Ni/YSZ anodes the low frequency process clearly behaves like a gas transport phenomenon (almost no temperature dependency, not influenced by H_2S), which is thus the most likely explanation. The medium frequency process is more pronounced than on Ni/GDC – it appears to be related to a classical electrochemical or electro-catalytic anode process. For further clarifying the nature of observed anode processes a modification of the anode microstructure (mainly an optimization of porosity) in conjunction with measurements on model-type thin film anodes need to be done.

Finally, a successful implementation of a Ni/GDC anode into a single metal-supported fuel cell could be demonstrated with a maximum power density of 0.88 Wcm^{-2} at 850 °C and in dry H_2. These results are very promising since this is – to the best of our knowledge – the first time that a particle-route-based Ni/GDC anode was implemented in a metal-supported SOFC and the performance already matches Plansee's current state-of-the-art MSC anode even at a first shot without extensive processing development. Moreover, the novel Ni/GDC anode exhibits a large optimization potential in terms of microstructure.

In conclusion, the replacement of YSZ by GDC in the cermet is a highly promising approach for obtaining porous anodes with increased electrochemical performance. Significant performance increase appears to be realistically achievable by further optimization of the anode's microstructure with special focus on enhancing the gas transport within pores.

Acknowledgements

Parts of the work were done in cooperation with the Christian Doppler Laboratory for Interfaces in Electrochemical Energy Converters. Christian Doppler Laboratories are funded in equal shares by the public authorities and the companies directly involved in the laboratories. The most important funding source of the public authorities is the Austrian Bundesministerium für Wissenschaft, Forschung und Wirtschaft (BMWFW). The funding is gratefully acknowledged.

References

[1] M.C. Tucker, Progress in metal-supported solid oxide fuel cells: a review, J. Power Sources 195 (2010) 4570–4582.
[2] D. Roehrens, F. Han, M. Haydn, W. Schafbauer, D. Sebold, N.H. Menzler, H.P. Buchkremer, Advances beyond traditional SOFC cell designs, Int. J. Hydrogen Energy 40 (2015) 11538–11542.
[3] M. Rüttinger, R. Mücke, Th Franco, O. Büchler, N.H. Menzler, A. Venskutonis, Metal-supported cells with comparable performance to anode-supported cells in short-term stack environment, ECS Trans. 35 (1) (2010) 259–268.
[4] Th Franco, R. Mücke, M. Rüttinger, N.H. Menzler, L.G.J. de Haart, A. Venskutonis, Lucerne: 9th european SOFC forum, metal-supported cells for mobile applications, Proceedings B802 (2010).
[5] M. Haydn, K. Ortner, Th Franco, O. Büchler, N.H. Menzler, A. Venskutonis, L. Sigl, Development of metal supported solid oxide fuel cells based on a powder metallurgical manufacturing route, Powder Metall. 56 (2013) 382–387.
[6] J.R. Wilson, S.A. Barnett, Solid oxide fuel cell Ni-YSZ anodes: effect of composition on microstructure and performance, electrochem, Solid State Lett. 11 (10) (2010) B181–B185.
[7] D. Simwonis, F. Tietz, Nickel coarsening in annealed Ni/8YSZ anode substrates for solid oxide fuel cells, Solid State Ionics 132 (3–4) (2010) 241–251.
[8] J. Ortner, M. Birkholz, T. Jung, New developments in hollow cathode gas flow sputtering, Vakuum Forschung und Praxis 15 (5) (2003) 236–239.
[9] S. Tang, U. Schulz, Gas flow sputtering - an approach to coat complex geomertries and non line of sight areas, Surf. Coat. Technol. 204 (6–7) (2009) 1087–1091.
[10] S. Uhlenbruck, N. Jordan, D. Sebold, H.P. Buchkremer, V.A.C. Haanappel, D. Stöver, Thin film coating technologies of (Ce,Gd)O2-d interlayers for application in ceramic high-temperature fuel cells, Thin Solid Films 515 (2007) 4053–4060.
[11] D.K. Niakolas, Sulfur poisoning of Ni-Based anodes for solid oxide fuel cells in H/C-Based fuels, Appl. Catal. 486 (2014) 123–142.
[12] L. Zhang, S.P. Jiang, H.Q. He, X. Chen, J. Ma, X.C. Song, A comparative study of H2S poisoning on electrode vehavior of Ni/YSZ and Ni/GDC anodes of solid oxide fuel cells, Int. J. Hydrogen Energy 35 (22) (2010) 12359–12368.
[13] S. Kavurucu Schubert, M. Kusnezoff, A. Michaelis, S.I. Bredikhin, Comparison of the performances of single cell solid oxide fuel cell stacks with Ni/8YSZ and Ni/10CGO anodes with H2S containing fuel, J. Power Sources 217 (2012) 364–372.
[14] W.C. Chueh, Y. Hao, W.C. Jung, S.M. Haile, High electrochemical activity of the oxide phase in model Ceria-Pt and Ceria-Ni composite anodes, Nat. Mater. 11 (2012) 155–161.
[15] T. Nakamura, K. Yashiro, A. Kaimai, T. Otake, K. Sato, T. Kawada, J. Mizusaki, Determination of the reaction zone in gadolinia-doped ceria anode for solid oxide fuel cell, J. Electrochem. Soc. 155 (12) (2008) B1244–B1250.
[16] V. Rojek, D. Röhrens, M. Brandner, N.H. Menzler, O. Guillon, A.K. Opitz, M. Bram, Development of high performane anodes for metal-supported fuel cells, ECS Trans. 68 (1) (2015) 1297–1307.
[17] T. Franco, M. Brandner, M. Rüttinger, G. Kunschert, A. Venskutonis, L.S. Sigl, Recent developments aspects of metal supported thin-film SOFC, ECS Trans. 25 (2) (2009) 681–688.
[18] M. Haydn, K. Ortner, T. Franco, S. Uhlenbruck, N.H. Menzler, D. Stöver,

G. Bräuer, A. Venskutonis, L.S. Sigl, H.P. Buchkremer, R. Vaßen, Multi-layer thin-film electrolytes for metal supported solid oxide fuel cells, J. Power Sources 256 (2014) 52–60.
[19] V. Esposito, D.W. Ni, Z. He, W. Zhang, A.S. Prasad, J.A. Glasscock, C. Chatzichristodoulou, S. Rasmousse, A. Kaiser, Enhanced mass diffusion phenomena in highly defective doped ceria, Acta Mater. 61 (2013) 6290–6300.
[20] F. Teocoli, V. Esposito, Viscoelastic properties of doped-ceria under reduced oxygen partial pressure, Scr. Mater. 75 (2014) 82–85.
[21] V. Duboviks, R.C. Maher, M. Kishimoto, L.F. Cohen, N.P. Brandon, G.J. Offer, A Raman spectroscopic study of the carbon deposition mechanism of Ni/CGO electrodes during CO/CO_2 electrolysis, Phys. Chem. Chem. Phys. 16 (26) (2014) 13063–13068.
[22] A. Tsoga, A. Gupta, A. Naoumidis, P. Nikolopoulos, Gadolinia-Doped Ceria and Yttria Stabilized Zirconia interfaces: regarding their application for SOFC technology, Acta Mater. 48 (18–19) (2000) 4709–4714.
[23] P. Costamagna, P. Costa, V. Antonucci, Micro-modelling of solid oxide fuel cell electrodes, Electrochimica Acta 43 (3–4) (1998) 375–394.
[24] F.S. Baumann, J. Fleig, H.U. Habermeier, J. Maier, Impedance spectroscopic study on well-defined (La,Sr)(Co,Fe)O3-d model electrodes, Solid State Ionics 177 (11–12) (2006) 1071–1081.
[25] S. Primdahl, M. Mogensen, Mixed conductor anodes: Ni as electrocatalyst for hydrogen conversion, Solid State Ionics 152–153 (2002) 597–608.
[26] A.K. Opitz, J. Fleig, Inverstigation of O_2 reduction on Pt/YSZ by means of thin film microelectrodes: the geometry dependence of the electrode impedance, Solid State Ionics 181 (2010) 684–693.
[27] M.P. Hoerlein, A.K. Opitz, J. Fleig, On the variability of oxygen exchange kinetics of platinum model electrodes on yttria stabilized zirconia, Solid State Ionics 247–248 (2013) 56–65.
[28] W. Lai, S.M. Haile, Impedance spectroscopy as a tool for chemical and electrochemical analysis of mixed conductors: a case study of ceria, J. Am. Ceram. Soc. 88 (11) (2005) 2979–2997.
[29] J. Jamnik, J. Maier, Generalised equivalent circuits for mass and charge transport : chemical capacitance and its implications, Phys. Chem. Chem. Phys. 3 (2001) 1668–1678.
[30] A. Bieberle, L.P. Maier, L.J. Gauckler, The electrochemistry of Ni pattern anodes used as solid oxide fuel cell model electrodes, J. Electrochem. Soc. 148 (6) (2001) A646–A656.
[31] A. Utz, H. Störmer, A. Leonide, A. Weber, E. Ivers-Tiffée, Degradation and relaxation effects of Ni patterened anodes in H2-H2O atmosphere, J. Electrochem. Soc. 157 (6) (2010) B920–B930.
[32] W.C. Chueh, W. Lai, S.M. Haile, Electrochemical behavior of ceria with selected metal electrodes, Solid State Ionics 179 (21–26) (2008) 1036–1041.
[33] P. Velicsanyi, M. Gerstl, A. Nenning, H. Hutter, J. Fleig, A.K. Opitz, The effect of Mn Co-doping on the electrochemical properties of Gd0.2Ce0.8O1.9-δ/Pt model-composite electrodes, ECS Trans. 68 (1) (2015) 1509–1516.
[34] P. Kim, D.J.L. Brett, N.P. Brandon, The effect of water content on the electrochemical impedance response and microstructure of Ni-CGO anodes for solid oxide fuel cells, J. Power Sources 189 (2) (2009) 1060–1065.
[35] J. Fleig, J. Maier, The influence of current constriction on the impedance of polarizable electrodes, J. Electrochem. Soc. 144 (11) (2007) L302–L305.
[36] A.K. Opitz, A. Lutz, M. Kubicek, F. Kubel, H. Hutter, J. Fleig, Investigation of the oxygen exchange mechanism on Pt/Yttria stabilized zirconia at intermediate temperatures: surface path versus bulk path, Electrochimica Acta 56 (2011) 9727–9740.
[37] J. Mizusaki, K. Amano, S. Yamauchi, K. Fueki, Electrode reaction at Pt, O_2 (g)/Stabilized zirconia interfaces, Part 1: theoretical consideration of reaction model, Solid State Ionics 22 (1987) 313–322.
[38] J. Mizusaki, K. Amano, S. Yamauchi, K. Fueki, Electrode reaction at Ot, O_2(g)/Stabilized zirconia interfaces, Part 2: electrochemical measurements and analysis, Solid State Ionics 22 (1987) 323–330.
[39] M. Gerstl, A. Nenning, R. Iskandar, M. Bram, A.K. Opitz, The sulphur poisoning behaviour of gadolinia doped ceria model systems in reducing atmospheres, Materials (2016) (accepted for publication).
[40] M.C. Doppler, J. Fleig, A.K. Opitz, The influence of sulfur poisoning and YSZ substrate orientation on electrochemical properties of nickel pattern anodes, ECS Trans. 68 (1) (2015) 1383–1390.
[41] J.F.B. Rasmussen, A. Hagen, The effect of H_2S on the performance of Ni–YSZ anodes in solid oxide fuel cells, J. Power Sources 191 (2) (2009) 534–541.
[42] C. Lee, J. Bae, Fabrication and characterization of metal-supported solid oxide fuel cells, J. Power Sources 176 (2008) 62–69.
[43] R. Férnandez-González, E. Hernández, S. Savvin, P. Núnez, A. Makradi, N. Sabaté, J.P. Esquivel, J.C. Ruiz-Morales, A novel microstructure metal-supported solid oxide fuel cell, J. Power Sources 272 (2014) 233–238.
[44] T. Klemenso, J. Nielsen, P. Blennow, A.H. Persson, T. Stegk, B.H. Christensen, S. Sonderby, High performance metal-supported solid oxide fuel cells with Gd-Doped ceria barrier layers, J. Power Sources 196 (2011) 7117–7125.
[45] P. Blennow, J. Hjelm, T. Klemenso, S. Rasmousse, A. Kromp, A. Leonide, A. Weber, Manufacturing and characterization of metal-supported solid oxide fuel cells, J. Power Sources 196 (2011) 7117–7125.
[46] P. Blennow, J. Hjelm, T. Klemenso, A.H. Persson, S. Rasmousse, M. Mogensen, Planar metal-supported SOFC with novel cermet anode, Fuel Cells 11 (5) (2011) 661–668.
[47] J. Nielsen, T. Klemenso, P. Blennow, Detailed impedance characterization of a well performing and durable Ni:CGO infiltrated cermet anode for metal-supported solid oxide fuel cells, J. Power Sources 219 (2012) 305–316.